FOURTH EUROPEAN ROTORCRAFT AND POWERED LIFT AIRCRAFT FORUM

Paper No. 7

AERODYNAMICS OF WING-SLIPSTREAM INTERACTION ESPECIALLY FOR V/STOL CONFIGURATIONS

B. Sträter
Institut für Flugtechnik
Technische Hochschule Darmstadt
Darmstadt, Germany

September 13 ÷ 15, 1978
STRESA - ITALY

Associazione Italiana di Aeronautica ed Astronautica
Assoziazione Industrie Aerospaziali

AERODYNAMICS OF WING-SLIPSTREAM INTERACTION ESPECIALLY FOR V/STOL CONFIGURATIONS

B. Sträter

Institut für Flugtechnik, Technische Hochschule Darmstadt

Abstract

A method for calculating the wing loading of propeller-wing-configurations is presented. The non-uniform velocity field within a slipstream is taken into account as well as displacement effects of an inclined slipstream occurring in the transition flight of a tilt wing V/STOL aircraft. A semiempirical procedure, describing the wing loading allows solutions even in the stalled region.

In calculating the aerodynamic characteristics of a propeller-slipstream configuration, the slipstream boundary conditions and the wing tangency flow condition are fulfilled.

Some results, showing the influence of the non-uniform slipstream velocity distribution are presented. In addition some predicted results are compared with test results.

1. Notation

a,b,c,d	coefficients of infinite series solution for velocity potential
C_D	drag coefficient
C_L	lift coefficient
C_m	pitching moment coefficient
C_N	normal force coefficient
C_T	thrust coefficient
C_{T_r}	resultant thrust coefficient
l	chord length
p	static pressure
R_P	propeller radius
R	fully contracted slipstream radius
u,v,w	velocity components in cartesian coordinates
V_∞	free stream velocity
V_Θ	swirl velocity
x,y,z	cartesian coordinates
x,r,φ	cylindrical coordinates
x_p	control point location
x_v	vortex point location
$\bar{x},\bar{r},\bar{y}$	dimensionless coordinates $\bar{x}=x/R$; $\bar{r}=r/R$; $\bar{y}=y/R$
Γ	circulation
Φ	velocity potential
α	angle of attack
δ	slipstream inclination angle in the Trefftz-plane
ε	downwash angle
λ	advance ratio
γ	dimensionless circulation
∇	effective turbulent viscosity

2. Introduction

The aerodynamic problem of the interaction between a wing and a propeller slipstream in which the wing is partially immersed is one of the prime considerations in the development of propeller-driven tilt-wing V/STOL aircraft. In contrast to conventional aircraft, the propulsion system of V/STOL aircraft is an integral part of the lifting system and wing-propeller interactions are used to achieve efficient and controllable transition flight. In this flight region between hover and cruise, the large inclination of slipstreams and the high angle of attack of the wing are remarkable. Figure 1 shows the predicted curves of the tilt angle and the wing angle of attack within the slipstreams over take-off and landing speed respectively. Furthermore, the propeller diameters are very large and most parts of the wings are immersed in the slipstreams. In the determination of the induced flowfield on the immersed wing parts, one has to care for the non-uniformity of the slipstream velocity distribution.

The present investigation reported herein was undertaken to define more exactly the effect of slipstream distribution on wing performance and to give a further insight into the stall charakteristics of the slipstream immersed wing.

At first, an actuator disc analysis for an inclined non-uniform slipstream is developed, then a non-linear semiempirical lifting line procedure is introduced. This method is valid for wings of moderate to high aspect ratio to which lifting line theory may be applied, but it is possible to obtain results in the separated flow region until and beyond maximum lift. At last, a superposition of these methods, both based on potential theory, will be realized, in order to obtain a tool for describing wing-slipstream interaction.

3. Propeller Analysis

The application of a propeller-slipstream procedure in a wing-slipstream interaction calculation for V/STOL aircrafts requires certain preconditions. Firstly, the model should describe the most important influences caused by the slipstream on the flowfield of the wing. The non-uniform axial slipstream velocity produces an increase in local velocity over the slipstream-immersed portion of the wing, while propeller swirl and displacement effect of the slipstream inclination change the wing local angle of attack. Secondly, the procedure should not be too difficult because the analytical and numerical problems in obtaining a wing-slipstream interaction solution are great enough. Therefore, complex vortex methods, as used in rotor dynamics, are out of question.

Here, an inclined actuator disc theory is combined with a twodimensional potential formulation.
The following assumptions have to be made:

- the flowfield is incompressible
- the slipstream cross section remains circular, even in a large distance downstream
- on the propeller disc the resultant force is the thrust also with inclination. The in-plane force which is usually small compared with the normal force is neglected
- the number of propeller-blades is infinite, then the loading of the propeller is a function of the radius r only and not of the angle of rotation φ.

If the radial loading is descretized concentric tubes with constant loading will be formed, as to be seen in the figure below.

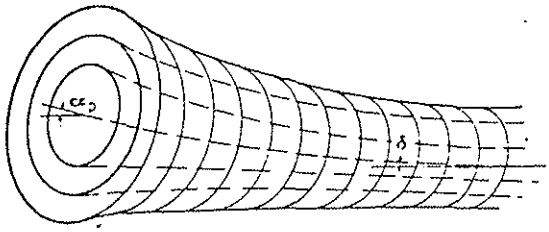

Slipstream Model

In a further simplification, the induced flowfield of an inclined propeller is only considered far behind the propeller disc, in the so-called Trefftz-plane. Then the problem becomes two-dimensional. In this plane, the radius of the greatest tube is taken as that of the fully contracted slipstream.

A slipstream coordinate system x,r, is introduced, as to be seen in the next figure. The x-axis is coincident with the tube axis. The propeller axis is inclined to the free-stream direction by an angle α_p, while the slipstream axis in the Trefftz-plane is inclined by an angle δ.

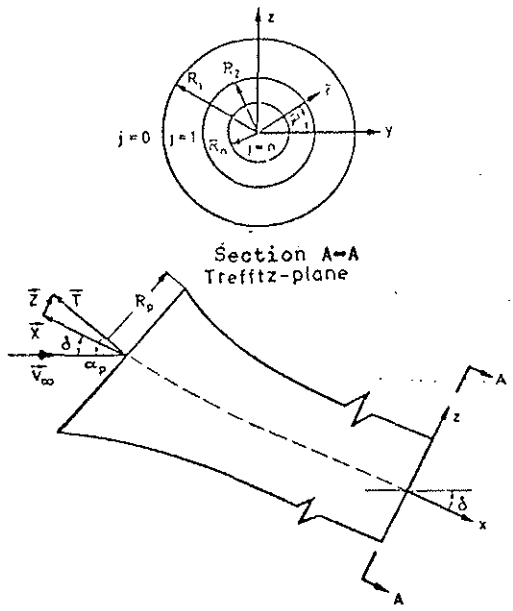

Coordinate System and Slipstream Geometry

On the slipstream boundary, two boundary conditions have to be fulfilled, the pressure and the flow angle condition. On the boundaries separating the different zones between j=1 and j=n (see figure above) the pressure and the flow angle condition have to be fulfilled, too. If the flowfield within each tube as well as outside the slipstream is inviscid and irrotational a velocity potential exist. Then the flowfield in each tube may be described by the La-place-equation

$$\Phi_{rr_j} + \frac{1}{r}\Phi_{r_j} + \frac{1}{r^2}\Phi_{\varphi\varphi_j} = 0 \qquad j=0,\ldots,n \quad .$$

The general solution of this equation is given by

$$\Phi_j(r,\varphi) = \sum_{m=0}^{\infty} (a_{m_j}\cos m\varphi + b_{m_j}\sin m\varphi)(C_{m_j} r^m + d_{m_j} r^{-m})$$

$$\text{for } r_{j+1} \leq r \leq r_j \text{ and } j=0,\ldots,n \quad .$$

The special solution of the velocity potential Φ_j is obtained by satisfying the two boundary conditions on each boundary surface mentioned above, and in addition the condition, that Φ_j outside the slipstream tends to zero as r tends to infinity and the condition that in the central tube Φ_n is finite on the slipstream centerline. The symmetric flow character with respect to the y- and z-plane simplifies the solution.

The velocity potential is a function of the Trefftz-plane-characteristics, the propeller induced axial velocities u_j, the inclination angle δ and the fully contracted slipstream radius R. Normally, the propeller radius R_p, the tilt angle α_p and the thrust distribution $C_T(r)$ are known. The combination of these variables is possible because of the conservation laws of mass, energy, and momentum (see (1)).

To calculate the wing loading of a propeller-wing-configuration, it is important to know the induced downwash due to the slipstream. In the aerodynamic coordinate system, the downwash angle is defined as

$$\varepsilon(r,\varphi) = -\arctan \frac{(w_j + |\vec{V}_\infty| \sin\delta)\cdot\cos\delta - u_j \sin\delta}{(w_j + |\vec{V}_\infty| \sin\delta)\cdot\sin\delta + u_j \cos\delta} \quad .$$

Figure 2 shows predicted downwash angles on the lateral axis of the slipstream with different thrust loadings $C_T(r)$. Within the slipstream downwash exists, while outside upwash can be recognized. The downwash angle equation shows that mainly the velocity components w_j and u_j influence the downwash angle. The thrust distributions may be expressed by the velocity distributions u_j, therefore, the great influence of the thrust loading is in reality the influence of the different velocity distributions u_j. The constant loading (curve a) agrees with a homoenergetic description of the slipstream as done by Levinsky e.a. (2).

In the slipstream centerline w_n is identical zero, therefor the downwash is only impressed by the axial velocity u_n. The results are shown in figure 3. In the past, except by Levinsky (2), authors often used a solid cylinder approximation in treating inclined slipstreams. This approximation is identical with the results of the thrust $C_{Tr} = \infty$. Especially the comparison with measurements in figure 4 shows that this approximation cannot be applied for small thrust values in the region of high angles of attack, while the present procedure gives a good agreement with the experimental data.

4. Lifting Line Analysis

Figure 1 has shown that especially in the landing phase the local geometric wing angle of attack within the slipstream may be in a region where flow separation occurs. The wing parts, not immersed in the slipstream have a local geometric angle of attack similar to the tilt angle, these parts are stalled during most of the period of transition. For predicting the aerodynamic characteristics of a V/STOL-aircraft, a method is necessary which also in the stalled region forces results.

Sivells (5) has first developed a non-linear lifting line procedure based on Prandtl's lifting line analysis using non-linear section lift data. It is an iterative procedure calculating the effective angle of attack with lifting line theory and comparing it with the given two-dimensional data for the airfoil sections incorporated in the wing.

For the calculation of wing-slipstream configurations Prandtl's lifting line theory has too many limitations for there is no fulfillment of the tangency flow condition, the restriction to high aspect ratio wings, and others.

Therefore a method was developed also using non-linear section data, but going out from an extended lifting line theory, published by Weissinger (4). Here the wing loading is replaced by a single lifting line located in the quarter-chord line. The flow tangency condition is fulfilled in the three quarter-chord line. This method is also applicable to swept wings and wings of moderate aspect ratios.

In the following swept wing are not considered because the use of section profile data only describes the local stall behaviour for rectangular wings of moderate or high aspect ratios.

Considering the local downwash in the sense of the three-quarter-chord theorem, Biot-Savart-law gives the following equation

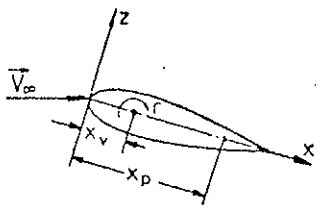

$$x_p = \frac{c_L \, l}{4\pi \tan\alpha} + x_v$$

If the angle of attack is small and $C_{L\alpha}$ is equal to 2π, the distance between the bound vortex Γ and the control point is a half chord (as in Weissinger's theory). In the stalling region, the lift gradient $C_{L\alpha}$ becomes smaller than 2π and the distance $x_p - x_v$ will vary as to be seen in the equation above.

In the linear theory the bound vortex Γ is placed in the aerodynamic center, which is defined by the following equation

$$\frac{x_{ac}}{l} = - \frac{dc_m}{dc_N} \quad .$$

In attached flow the aerodynamic center on profiles is near the quarter chord point. With the onset of separation the pressure distribution changes significantly. An aerodynamic center with a definition as above is no more well-defined. The origin of force moves backwards. Therefore, in this case, the bound vortex is placed in a so-called vortex point. This point is under all flow conditions the origion of the resultant normal force, its position is defined by the equilibrium of pitching moment. The vortex point definition follows than to be

$$\frac{x_v}{l} = - \frac{c_m - c_{mo}}{c_N} \quad .$$

If the two-dimensional aerodynamic characteristics and the local effective angle of attack are known the local vortex point may be calculated. In the linear angle of attack range aerodynamic center and vortex point location are identical. In the limiting case of high angles of attack with complete flow separation, the origin of the normal force is nearly at a half chord. For c_{m_o} is usually much smaller than c_m in this case, the vortex point is situated in the center of pressure

$$\frac{x_{c\,p}}{l} = - \frac{c_m}{c_N} \quad .$$

The position of the vortex point depends on the local lift coefficient and the local circulation respectively, therefore the lifting line integral equation becomes non-linear. To obtain a solution, a discrete horseshoe vortex representation is used for the wing. The solution is performed numerically in an iterative manner. The following non-linear set of equation is obtained. For

the flow tangency condition which is fulfilled just between the two free vortices of a horseshoe vortex

$$\tan\alpha = -\frac{w_i}{V} = \sum_{h=1}^{\bar{m}} J_{hi}\,\gamma_h \quad .$$

The downwash on the location i is obtained by summing over the downwash elements of the $\bar{m}$ horseshoe vortices. The correlation function J_{hi} describing the geometric assignment of vortex and control points depends on the dimensionless circulation γ, therefore the equations are non-linear.

To handle the equation, a solution in the linear range is calculated at first. Then the location of the local bound vortices and the control points are corrected using the two-dimensional airfoil data at an effective angle of attack equal to the local geometric angle of attack less the induced angle of attack. Thereby the correlation function J_{hi} is changed and a new solution vector γ is obtained. The iteration procedure ends if either convergence is obtained or if a maximum number of iterations has been performed.

The figures 5 and 6 show some of the results. In figure 5 the position of the bound vortices and the control points of a rectangular wing of an aspect ratio of 5 are to be seen. In the attached flow regime up to 10° angle of attack the locations of bound vortices and control points are in the well-known position of quarter-chord and tree-quarter chord line respectively. With increasing flow separation at higher angles of attack the control points x_p move forward while the positions of the bound vortices move rearward. With increasing angle of attack the stall progression from the inner part of the wing to the outer part is noticable.

In figure 6 predicted and measured lift and drag curves are compared. The conformity in lift even in the stall region is very well. As far as drag characteristics are concerned, the profile drag from the two-dimensional profile data is taken into account too, therefore the conformity in drag is also very well.

5. Wing-Slipstream-Interaction

With the slipstream model presented in chapter 3 and the wing theory introduced in chapter 4 tools are prepared for claculating the loading of a wing partly or fully immersed in a slipstream.

A simple potential superposition of the wing and slipstream calculation is impossible. The wing-vortex system induces a flowfield, violatine the boundary conditions of the slipstream surfaces; on the other hand the slipstream vortex system breaks the tangency flow condition on the wing. In the interaction calculation the slipstream as well as the wing boundary conditions have to be considered once more.

The condition that the flow inclination adjacent to the tube boundaries must be the same on both sides, may be written

$$\vec{V}_{j-1} \times \vec{V}_j \cdot \vec{e}_{\varphi}\,(R_j,\varphi,x) = 0$$

With the assumption that the perturbation velocity in x-direction is small compared with the axial slipstream component ($\partial\phi/\partial x \ll u$); this equation leads to

$$\frac{\partial\Phi_j}{\partial r} = \frac{u_j}{u_{j-1}}\,\frac{\partial\Phi_{j-1}}{\partial r} + w_{\infty}\cdot\sin\varphi\,\left(\frac{u_j}{u_{j-1}} - 1\right) \quad \text{for } r=R_j \quad .$$

The interference of the wing vortex system results in a radial velocity jump on each surface. This velocity jump can be produced by a distribution of sources and sinks on the boundaries (see (1)).

Secondly, the pressure must be the same on both sides of a slipstream boundary surface

$$p_{j-1} = p_j \quad .$$

With the neglect of the second order perturbation elements the pressure condition leads to

$$\frac{\partial \Phi_j}{\partial x} = \frac{u_{j-1}}{u_j} \frac{\partial \Phi_{j-1}}{\partial x} \quad , \qquad \text{for } r=R_j$$

This axial velocity jump on each boundary surface can be produced by a distribution of lifting elements e.g. horseshoe vortices.

The additional distributions of sources and vortices on the tube surfaces fulfilling the boundary conditions are nothing but a great wasting of time. With the following definition of a new perturbation potential the source distribution can be eliminated and the numerical treatment of the interference problem can be simplified

$$\tilde{\Phi}_j = \frac{u_o}{u_j} \Phi_j + \frac{u_o}{u_j} w_\infty \sin\varphi \cdot r \quad , \quad \text{for} \quad R_{j+1} \leq r \leq R_j \quad .$$

For the special case of an axial flow this transformation changes over into a formula defined by Ribner (6) for an uniform slipstream.

With the foregoing transformation deliminating the source distribution an augmented axial velocity jump arises. This potential jump can be produced by a distribution of horseshoe vortices with the bound vortex situated in the propeller plane. The circulation Γ^p matches with the potential jump over the boundary surface

$$\Gamma_j^p = \Phi_{j-1} - \Phi_j \quad .$$

Futhermore, the resultant flow field of the wing including slipstream can be represented entirely in terms of this vortex distribution together with another vortex distribution over the wing and wake. Therefore the following equivalent singularity model for a wing-slipstream-configuration is obtained.

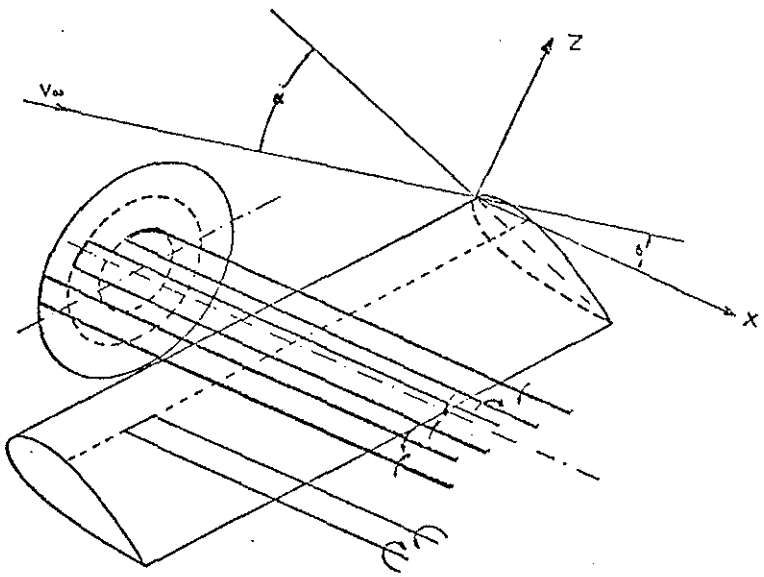

For the sake of clarity only one horseshoe vortex of each vortex system is shown.

Besides the slipstream boundary condition the flow tangency condition on the wing has to be fulfilled, too. With the neglect of the velocity components in y-direction this condition leads to the following equation

$$\bar{w}_j \cos(\alpha-\delta) - \bar{u}_j \sin(\alpha-\delta) = |\vec{V}_\infty| \sin\alpha \quad .$$

The velocity components $\bar{w}_j$ and $\bar{u}_j$ contain all perturbation increments occuring in the control points. E.g. $\bar{w}_j$ is summed from the wing downwash, from the downwash of all slipstream vortex systems, from the downwash of the slipstream inclination and within the slipstream of the velocity components in z-direction of the swirl velocity caused by the propeller rotation. A simple vortex model of the slipstream has been used to calculate this swirl velocity. However, in order to keep the velocity finite near the axis, the central vortex is softened by introducing viscous core effects in the following semiempirical manner

$$\frac{V_\Theta}{V_\infty} = \frac{\lambda}{2} \frac{C_{T_r}}{\bar{r}} \left(1 - e^{-\bar{r}^2 \frac{\sqrt{C_{T_r} \cdot \cos^2\delta}}{4\,\bar{r}\,\bar{x}}} \right) \quad .$$

Satisfying the two remaining boundary conditions, it is possible to calculate the unknown vortex distribution representing the tube surfaces and the wing and wake. The condition that the resultant flow velocity is tangent to the effective wing surface at the i'th control point leads to a series of equations of the form

$$\frac{w_i}{V_\infty} = \sum_{h=1}^{\bar{m}} \gamma_h^w J_{hi} + \sum_{f=1}^{o_r} \gamma_f^p J_{fi} \quad .$$

The elements J_{hi} represent the geometric attribution of the wing vortices γ^w to the i'th wing control point. The elements J_{fi} represent the geometric attribution of all tube vortices γ^p to the i'th wing control point. o_r is the resultant number of all tube vortices

$$o_r = K \sum_{j=1}^{n} o_j \quad ,$$

K points out of number of propeller.

The pressure condition also leads to a series of equations

$$\gamma_i^p = \text{const} \left(1 - \left(\frac{u_{j-1}}{u_j}\right)^2\right) \left\{ \sum_{h=1}^{\bar{m}} \gamma_h^w Q_{hi} + \sum_{f=1}^{o_r} \gamma_f^p Q_{fi} \right\} \quad ,$$

$$\text{for} \quad r = R_j \quad .$$

Here the elements Q_{hi} are describing the geometric relation of the wing vortices γ^w to the i'th tube control point, situated in the middle of the free vortices of a tube horseshoe vortex in the x-z-plane of the wing control points. Q_{fi} describes the geometric assignment between the tube vortices and the i'th tube control point.

The structure of both series of equations can be seen in the matrix-notation

$$(A)\ \{\gamma^w\} + (B)\ \{\gamma^p\} = \{f(\alpha)\}$$
$$(C)\ \{\gamma^w\} + (D)\ \{\gamma^p\} = 0 \quad .$$

This equation system is solved iteratively in the same manner as shown in chapter 3 for wing alone.

Some results are represented in the figures 7 - 10. Figure 7 shows the calculated influence of different non-uniform propeller loadings on the local lift curve. The three idealised loadings C_T = const; C_T = const·r and C_T = -const r were investigated. The integral loading was the same in all cases. The slipstream was divided into four tubes with uniform loading.

A significant influence of the propeller loading and of the propeller rotation being responsible for the unsymmetrical lift distribution within the slipstream can be recognized. This influence has been confirmed by experiments, as to be seen in figure 8. Measured and predicted lift distributions with a uniform disc loading and a non-uniform loading obtained from a measured dynamic pressure distribution within the slipstream are compared. The measured values especially near the slipstream axis can be better predicted with the non-uniform slipstream procedure.

The figures 9 and 10 show the comparison of measured and predicted integral lift and drag characteristics. In the lift and drag calculation of the wing alone there were some differences in comparison with the measured values, the reason was the propeller nacelle mounted on the wing tip. In order to obtain comparable results, the calculated curves were corrected in the following manner

$$C_L = \left(C_{L_{w.p.}} - C_{L_{wo.p.}}\right)_{Calculation} + \left(C_{L_{wo.p.}}\right)_{Measurement}.$$

The subscript w.p. denotes "with propeller" and wo.p. "without propeller".

The calculated lift and drag increment due to the slipstream was added to the measured values of the clean wing. The corrected curves are in a good conformity with the experiments even in the region of maximum lift.

6. Summary

In the present paper a method for calculating the loading and the aerodynamic characteristics of propeller-wing-configurations is presented. The procedure is limited to rectangular wings with moderate or high aspect ratios. In particular the non-uniform slipstream velocity field, the displacement effect of inclined slipstream and the non-linear behaviour of the wing in the high angle of attack region are considered.

The knowledge of the sectional profile data and the thrust distribution or the slipstream velocity distribution respectively is necessary.

The wing-propeller-interaction procedure fulfills the slipstream boundary conditions and the wing tangency flow condition.

Predicted results show a great influence of the non-uniform slipstream velocity field on the spanwise wing loading. Comparison with test data has shown that the theory predicts the span loading and downwash angle of an inclined slipstream reasonably well.

7. References

(1) B. Sträter, Ein Beitrag zum Problem der Propeller-Flügel-Interferenz, Doctoral Thesis, Technical University Darmstadt, 1976.

(2) E.S. Levinsky, H.U. Thommen, P.U. Yager and C.H. Holland, Lifting Surface Theory and Tail Downwash Calculations for V/STOL Aircraft in Transition and Cruise, Air Vehicle Corp. San Diego, Final Report 356, 1968.

(3) L.F.G. Simmons and E. Ower, Investigation of Downwash in the Slipstream, ARC R+M 882, 1923.

(4) J. Weissinger, Über eine Erweiterung der Prandtlschen Theorie der tragenden Linie, Mathematische Nachrichten, 2. Band, 1949.

(5) J. Sivells and R. Neely, Method for Calculating Wing Characteristics by Lifting-Line Theory Using Non-linear Section Lift Data, NACA TN 1269, 1947.

(6) H.S. Ribner, Theory of Wings and Slipstream, UTIA Rep. 60, 1959.

(7) B. Wagner und W. Siegler, Messungen zur Flügel-Höhenleitwerks Interferenz bis in den Bereich hoher Anstellwinkel für Flügel der Streckung 5 und verschiedener Pfeilung und Zuspitzung, Institutsbericht des Instituts für Flugtechnik der TH Darmstadt, 1971.

(8) M. George and E. Kisielowski, Investigation of Propeller Slipstream Effects on Wing Performance, Dynasciences Corp., Blue Bell, 1967.

(9) B. Sträter, Experimental and Theoretical Investigations on the Problem of Propeller-Wing Interference up to High Angles of Attack, NASA TT F-16490, 1975.

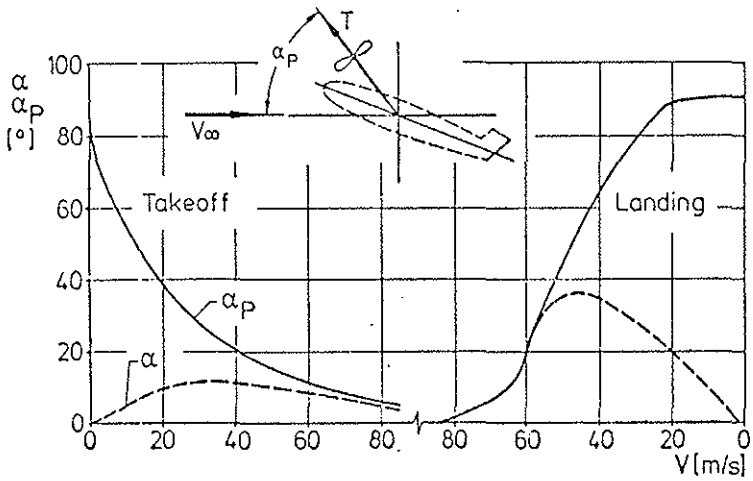

Fig. 1 Predicted Tilt Angle α_p and Wing Angle α of Attack of a Tilt Wing V/STOL Aircraft

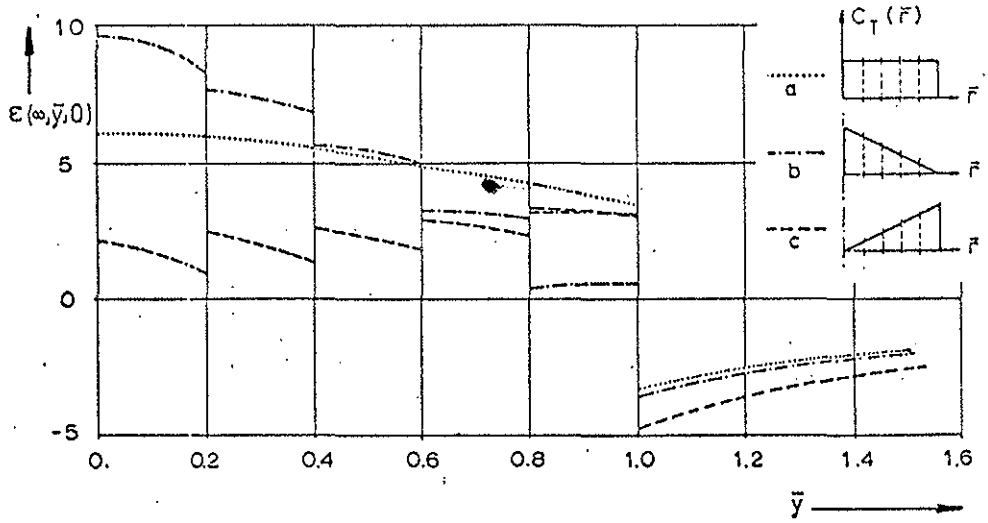

Fig. 2 Predicted Downwash Angle on Slipstream Lateral Axis $\alpha_p=30^o$ $C_{T_r}=1$

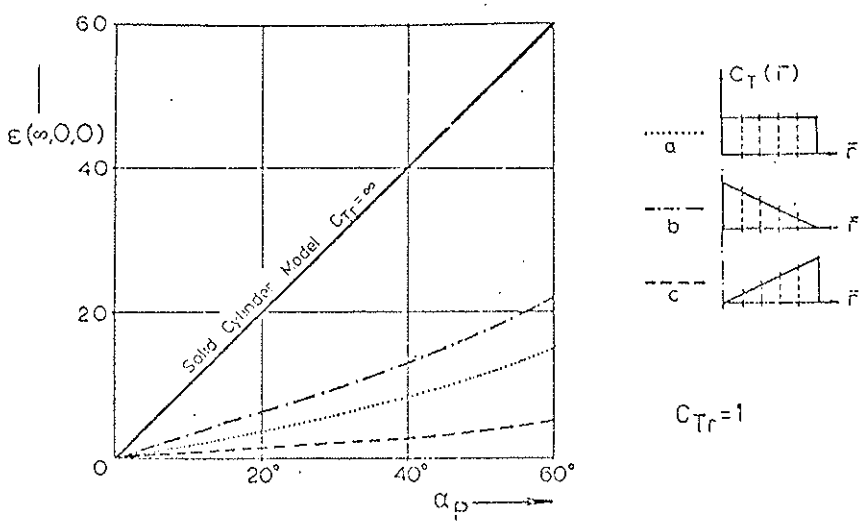

Fig. 3 Downwash Angle on Slipstream Centerline

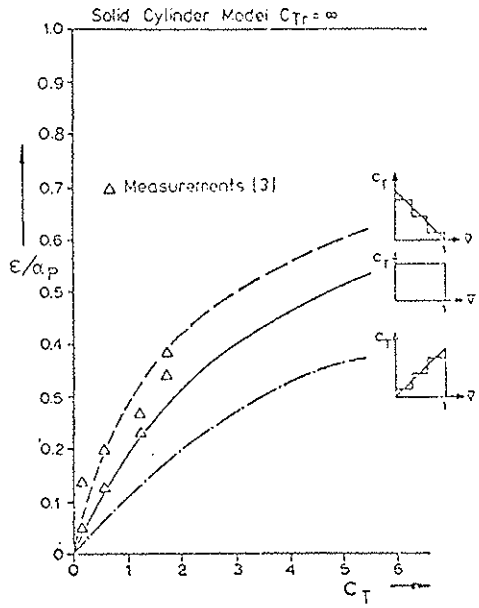

Fig. 4 Predicted and Measured Downwash on Slipstream Axis

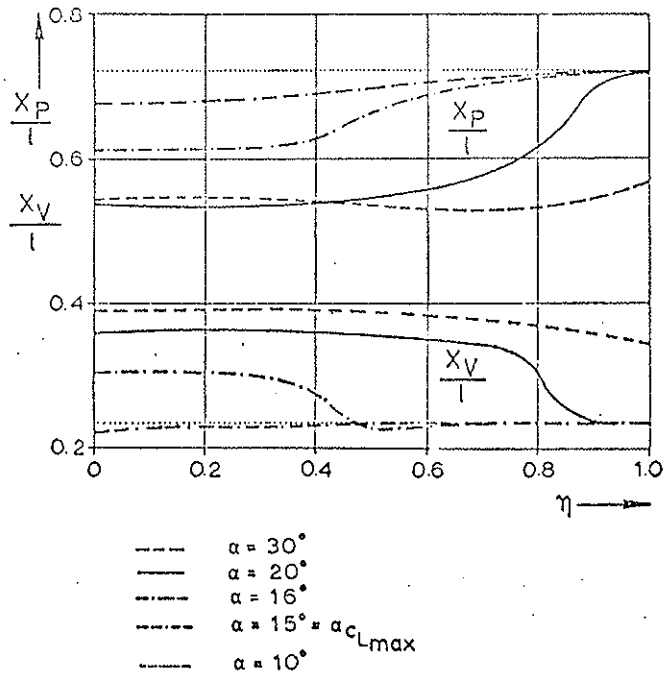

Fig. 5 Predicted Locations of Vortex- and Control-Points of a Rectangular Wing

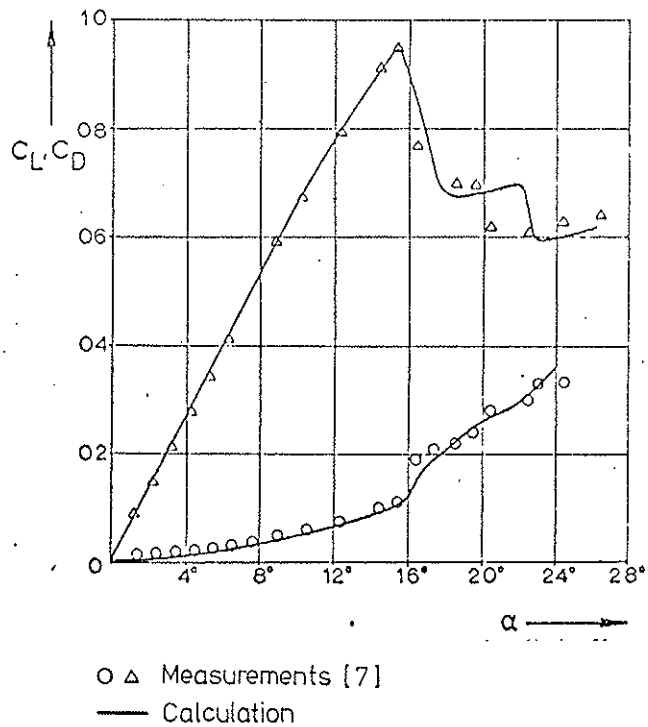

Fig. 6 Aerodynamic Characteristics of a Rectangular Wing $\mathfrak{AR}=5$ Profile NACA 0012 $Re=0.61\cdot10^6$

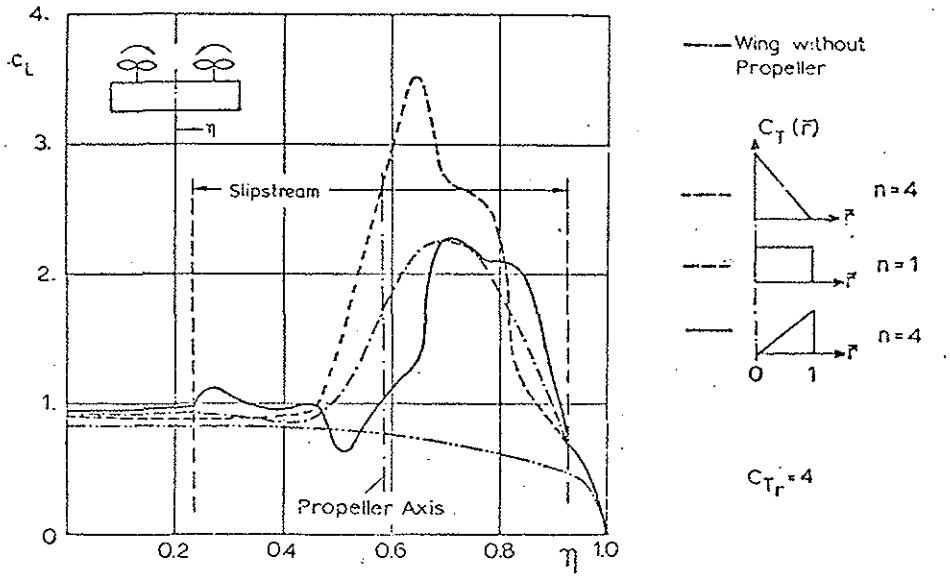

Fig. 7 Predicted Spanwise Loadings for a Rectangular Wing $\mathfrak{A}=3.26$ Profile NACA 4415

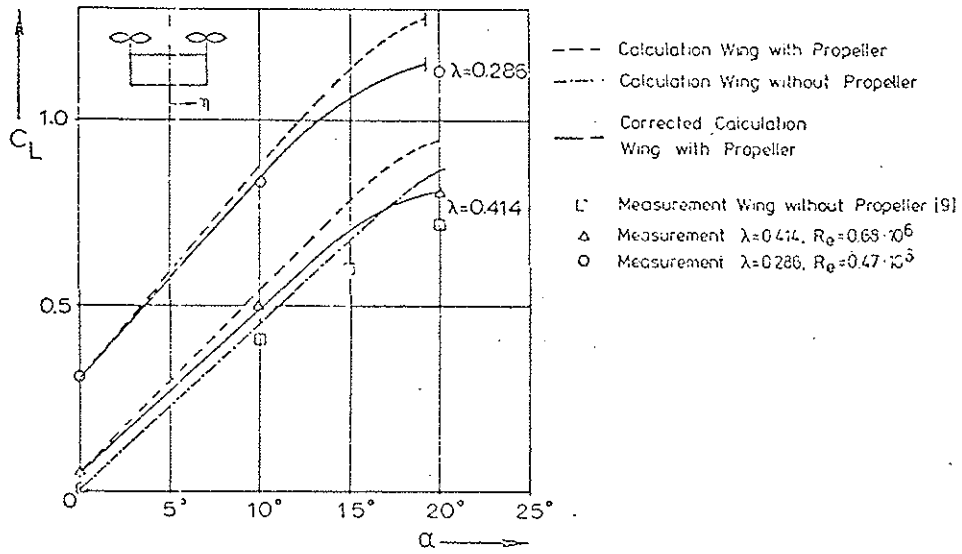

Fig. 9 Predicted and Measured Lift Characteristics $\mathfrak{A}=2.87$ Profile NACA 0018

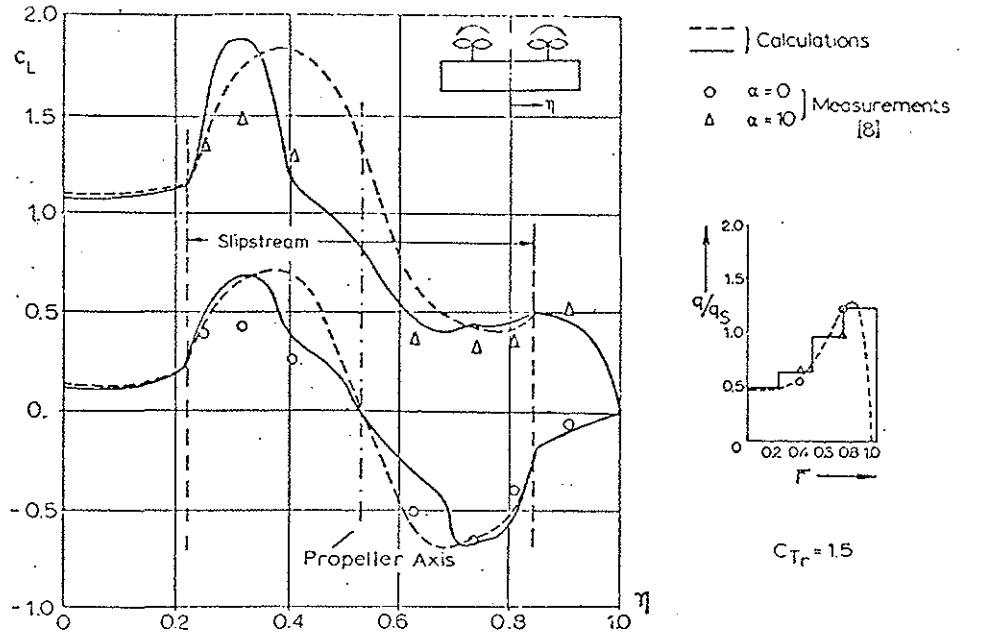

Fig. 8 Predicted and Measured Influence of a Non-Uniform Slipstream Velocity on Spanwise Loading $\mathfrak{A}=6.36$ Profile NACA 0015

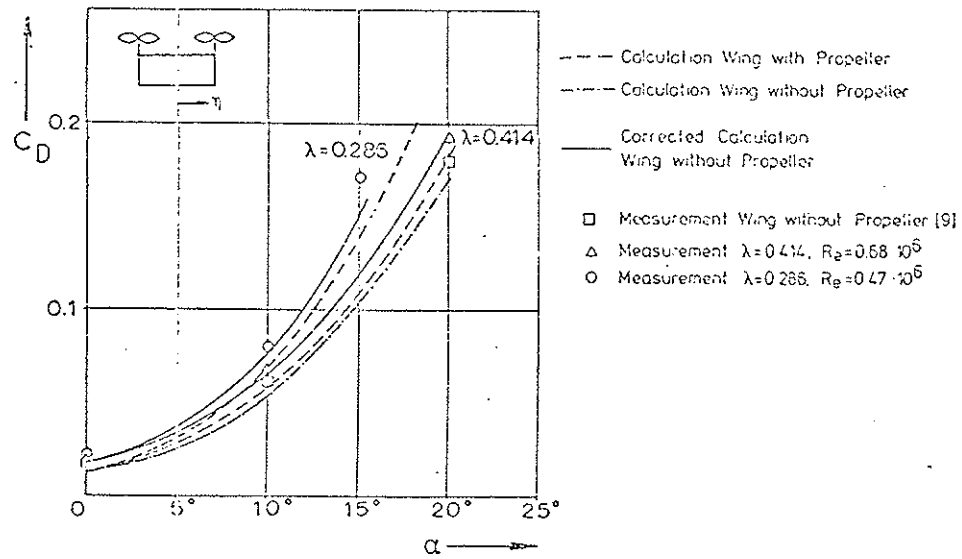

Fig. 10 Predicted and Measured Drag Characteristics $\mathfrak{A}=2.87$ Profile NACA 0018